Journal of Physics: Theories and Applications E-ISSN: 2549-7324 / P-ISSN: 2549-7316
J. Phys.: Theor. Appl. Vol. 9 No. 2 (2025) 198-212 doi: 10.20961/jphystheor-appl.v9i2.108563

Thermal and nonthermal behaviors of electron–H_2O in presence of laser field

Harish Bohara[1], Raju Bohora[2], Sharad Kumar Oli[2], Kishori Yadav[2], Santosh Kumar Das[2*], Saddam Husain Dhobi[2*]

[1]Department of Physics, Golden gate international college, Tribhuvan University, Kathmandu, Nepal
[2]Department of Physics, Patan Multiple Campus, Tribhuvan University, Patan Dhoka, Lalitpur, Nepal

Corresponding: saddam@ran.edu.np/dassantosh29@gmail.com

Received 28 August 2025, Revised 11 September 2025, Published 30 October 2025

Abstract: Electron–water (H_2O) molecule scattering under the influence of laser and thermal fields is a fundamental process in atomic and molecular physics, with significant implications for radiation chemistry, photonics, and quantum control. The interaction of electrons with H_2O in the presence of an external laser field modifies the scattering dynamics by introducing additional energy and momentum channels, while thermal effects influence electron oscillations and resonance behavior. Understanding these combined effects is essential for accurately predicting differential cross-sections (DCS) and controlling scattering probabilities in experimental and applied settings, including laser-assisted spectroscopy, nanostructure interactions, and thermally tunable quantum devices. The aim of this work is to study the nature of electron-H_2O in presence of laser and heat using scattering technique. For this we design a theorical model which include thermal wave function, potential of water molecules, S-matrix, Besel function and Kroll-Watson approximation for DCS. The developed model was computed used temperature (293–300 K), scattering angles (0.057°–57°), momentum transfer (0.3–1 eV), distance separation (1–1.5 Å), field strength (0.3–5 a.u.), relative field strength (0.5–2.5 a.u.), electron conductivity (0.1–15 a.u.), polarization (linear, circular, elliptical), and Bessel function order. The computed result shows thermal effects enhance DCS compared to non-thermal conditions (0 K), with resonances observed at specific energies (0.25–1 eV). Higher scattering angles produce larger DCS, while lower angles generate sharper resonances with damping-like behavior. Elliptical polarization yields the highest DCS, followed by circular and linear. Distance separation and electron conductivity modulate constructive and destructive interference patterns, whereas higher-order Bessel functions stabilize DCS, indicating equilibrium between electrostatic interaction and particle rest energy. These findings suggest that controlled temperature and field parameters can manipulate scattering probability in thermal systems.

Keywords: Electron–water, scattering, differential cross-sections, S-matrix, Besel function and Kroll-Watson approximation

1. Introduction

Electron collisions with atoms, molecules, and surface targets serve as crucial tools for probing and understanding processes in laboratory plasmas, astrophysics, and laser-driven systems (Bartschat et al., 2014). Gaining insight into the electronic structure of atoms and molecules is essential across physics, chemistry, and biology, where electron-impact ionization provides valuable information (De Avillez et al., 2019). One of the fundamental collision processes is the (e, 2e) reaction, in which an incident electron ionizes a target by ejecting a bound electron and subsequently scattering. The momenta of both the ejected and scattered electrons can be fully resolved experimentally, offering comprehensive data about the interaction (Campeanu et al., 2018). Complete characterization of such processes is given by the triple differential cross-section (TDCS), which describes the probability of detecting outgoing electrons with specific momenta. Over the years, significant progress has been made in measuring and theoretically modeling TDCS for various atomic and molecular systems (Colgan et al., 2002). In recent decades, laser-assisted electron collisions have received increasing attention due to their fundamental interest and applications in plasma physics and astrophysics, where scattering cross-section information is critical (Ehlotzky, 2001). Early theoretical approaches often ignored the dressing effects of the target, but these were later included by describing final states using Volkov or Coulomb-Volkov wavefunctions, revealing notable variations in differential cross-sections (Zarcone et al., 1983). A wide range of studies has since examined both single and double ionization of atomic targets under laser-assisted electron impact (Khalil et al., 1997).

Although significant studies have explored laser-assisted electron collisions and (e,2e) processes in atomic and molecular targets, research on electron–water scattering under combined laser and thermal effects remains limited. Most theoretical models focus on zero-temperature or monochromatic field conditions, neglecting the influence of finite temperatures on scattering dynamics. Additionally, the role of non-monochromatic laser fields and thermal oscillations in modifying DCS, resonance behavior, and interference patterns in electron–H_2O collisions is not well understood. Addressing these gaps is essential for accurately predicting scattering probabilities and for controlling electron–molecule interactions in thermal and applied laser-driven systems.

2. Methods and Materials

The off-shell LFA for potential scattering in a strong linearly polarized monochromatic laser field was derived in appendix A of paper M. This theory can be easily generalized to a laser field with an arbitrary vector potential A(t). The only condition which A(t) should satisfy is the $2\pi/\omega$-periodicity, where ω is the fundamental harmonic frequency. For example, the vector potential of a N-color elliptically polarized laser field has the form (Milosevic, 1996)

$$\mathrm{A(t)} = \mathrm{A_0} \sum_{n=1}^{N} a_n [\Lambda_{1\mathrm{n}} \cos(n\omega t + \varphi_n) + \Lambda_{2\mathrm{n}} \sin(n\omega t + \varphi_n)] \quad (1)$$

where $a_n, n\omega$ and φ_n are the relative amplitude (a is the ratio of field strength) (Luo et al., 2017), frequency and phase (phase $\phi = 0,\pi/4,\pi/2, 3\pi/4$ and π) of the n[th] vector potential component. The polarization of the nth component is defined by the vectors $\Lambda_{1n} = \hat{e}_1 cos\zeta_n$ and $\Lambda_{2n} = \hat{e}_2 sin\zeta_n$. For $\zeta_n = 0$ the n[th] component is linearly polarized, while for $\zeta_n = \frac{\pi}{4}$ the polarization is circular. A0 is equal field amplitude (Ehlotzky, 2001; Batra et al., 2024). The most notable gauges in strong-field physics beyond the dipole approximation are the Lorentz-gauge and the Coulomb gauge (Maurer & Keller, 2021; Kurmi et al., 2025).

$$\chi\,(r,t) = \frac{1}{(2\pi)^{3/2}} exp\left\{ i\frac{p}{\hbar}.\left(r + \frac{e}{m}\int \boldsymbol{A}(t')dt'\right) - i\frac{E}{\hbar}t - i\frac{e^2}{2m\hbar}\int \boldsymbol{A}^2(t')\,dt'\right\} \quad (2)$$

Substituting value of A from equation (1) and solving we get

$$\chi(r,t) = \frac{1}{(2\pi)^{3/2}} exp\left\{\left(i\boldsymbol{p}.\boldsymbol{r} + \sum_{n=1}^{N}\frac{ia_n\alpha_0 p\sin(n\omega t+\varphi_n-\gamma)}{n}\right) - iEt \right.$$
$$- i\frac{\alpha_0}{4}\sum_{n=1}^{N}\frac{\boldsymbol{a}_n}{n}\left[\Lambda_{1\mathrm{n}}^2\left\{n\omega t + \frac{\sin(2n\omega t+2\varphi_n)}{2}\right\}\right.$$
$$\left.\left. - \Lambda_{2\mathrm{n}}\Lambda_{1\mathrm{n}}\cos\big(2(n\omega t+\varphi_n)\big) + \Lambda_{2\mathrm{n}}^2\left\{n\omega t - \frac{\sin(2n\omega t+2\varphi_n)}{2}\right\}\right]\right\} \quad (3)$$

For thermal case we use superposition for thermal and laser field electron and an expression is desing as,

$$\chi\,(r,t) = \frac{1}{(2\pi)^{3/2}} exp\left\{\left(i\boldsymbol{p}.\boldsymbol{r} + \sum_{n=1}^{N}\frac{ia_n\alpha_0 p\sin(n\omega t+\varphi_n-\gamma)}{n}\right) - iEt \right.$$
$$- i\frac{\alpha_0}{4}\sum_{n=1}^{N}\frac{\boldsymbol{a}_n}{n}\left[\Lambda_{1\mathrm{n}}^2\left\{n\omega t + \frac{\sin(2n\omega t+2\varphi_n)}{2}\right\}\right.$$
$$\left.\left. - \Lambda_{2\mathrm{n}}\Lambda_{1\mathrm{n}}\cos\big(2(n\omega t+\varphi_n)\big) + \Lambda_{2\mathrm{n}}^2\left\{n\omega t - \frac{\sin(2n\omega t+2\varphi_n)}{2}\right\}\right]\right\}$$
$$- k_e\nabla\mathrm{T}\exp(\mathrm{i}\omega_{\mathrm{eT}}\mathrm{t}) \quad (4)$$

Since the complex conjugate of last term is zero so we neglect it and solving equation (4) with assuming $\frac{\hat{e}_2.\boldsymbol{p}}{\hat{e}_1.\boldsymbol{p}}\tan\zeta_n = \tan\gamma => \tan\theta\tan\zeta_n$ and $\gamma => \tan^{-1}(\tan\theta\tan\zeta_n)$ (Dhobi et al., 2025a) we get ,

$\chi_E\,(r,t)$

$$= \frac{1}{(2\pi)^{3/2}} exp\left\{\left(i\boldsymbol{p}.\boldsymbol{r} + \sum_{n=1}^{N}\frac{ia_n\alpha_0 p\sin(n\omega t+\varphi_n-\gamma)}{n}\right) - iEt\right\}$$
$$- k_e\nabla\mathrm{T}\exp(\mathrm{i}\omega_{\mathrm{eT}}\mathrm{t}) \quad (5)$$

Now to calculate the scattering matrix we have

$$S_{fi} = \delta_{fi} - \frac{i}{\hbar}\int_{-\infty}^{+\infty}\langle\chi_f(r,t)|V(r)|\chi_i(r,t)\rangle\,dt \quad (6)$$

Now putting the value form equation (5) and from equation (6) for spherical coordinate system we have

$$S = \delta_{fi} - \int\int \left[\frac{1}{(2\pi)^{3/2}} exp\left\{\left(-i\boldsymbol{p_f}.\boldsymbol{r} - \sum_{n=1}^{N} \frac{ia_n\alpha_0 p_f \sin(n\omega t + \varphi_n - \gamma)}{n}\right) + iE_f t\right\} - k_{ef}\nabla \mathrm{T_f} \exp(-\mathrm{i}\omega_{\mathrm{eTf}}\mathrm{t})\right] \mathrm{V(r)} \left[\frac{1}{(2\pi)^{3/2}} exp\left\{\left(i\boldsymbol{p_i}.\boldsymbol{r} + \sum_{n=1}^{N} \frac{ia_n\alpha_0 p_i \sin(n\omega t + \varphi_n - \gamma)}{n}\right) - iE_i t\right\} - k_{ei}\nabla \mathrm{T_i} \exp\,(\mathrm{i}\omega_{\mathrm{eTi}}\mathrm{t})\right] d^3r dt \quad (7)$$

$$S = \delta_{fi} - \int\int \frac{1}{(2\pi)^2} exp\left\{\left(-iqrcos\theta - \sum_{n=1}^{N} \frac{ia_n\alpha_0 q \sin(n\omega t + \varphi_n - \gamma)}{n}\right) + i\Delta E t\right\} \mathrm{V(r)} d^3r dt + \int\int k_{ei}\nabla \mathrm{T_i} \exp(\mathrm{i}\omega_{\mathrm{eTi}}\mathrm{t})\, exp\left\{\left(-ip_f rcos\theta - \sum_{n=1}^{N} \frac{ia_n\alpha_0 p_f \sin(n\omega t + \varphi_n - \gamma)}{n}\right) + iE_f t\right\} \mathrm{V(r)} d^3r dt + \int\int \frac{k_{ef}\nabla \mathrm{T_f} \exp(-\mathrm{i}\omega_{\mathrm{eTf}}\mathrm{t})}{(2\pi)^{3/2}} exp\left\{\left(ip_i rcos\theta + \sum_{n=1}^{N} \frac{ia_n\alpha_0 p_i \sin(n\omega t + \varphi_n - \gamma)}{n}\right) - iE_i t\right\} \mathrm{V(r)} d^3r dt - \int\int k_{ef}k_{ei}\nabla \mathrm{T_f}\nabla \mathrm{T_i} \exp\,(\mathrm{i}\omega_{\mathrm{eTi}}\mathrm{t} - \mathrm{i}\omega_{\mathrm{eTf}}\mathrm{t}) \mathrm{V(r)} d^3r dt \quad (8)$$

Where, $p_f - p_i = q$, $\Delta E = E_f - E_i$, As we have for N=1 and applying Besel function to equation (8) like equation (9) to other assuming $c_n = -\frac{a_n\alpha_0 q}{n}, c_{nf} = -\frac{a_n\alpha_0 f_f}{n}, c_{ni} = \frac{a_n\alpha_0 p_i}{n}$

$$e^{iz\sin(\theta)} = \sum_{m}^{\infty} J_m(z) e^{im\theta} \quad (9)$$

From equation (9) and equation (8) we have

$$S = \delta_{fi} - \int\int \frac{1}{(2\pi)^2} exp\{-iqrcos\theta + i\Delta Et\} \sum_m^{\infty} J_m(c_{nf})\, e^{\sum_{n=1}^{N} im(n\omega t+\varphi_n-\gamma)}\, \mathrm{V(r)} d^3rdt + \int\int k_{ei}\nabla \mathrm{T_i} \exp(\mathrm{i}\omega_{\mathrm{eTi}}\mathrm{t})\, exp\{-ip_f rcos\theta + iE_f t\} \sum_m^{\infty} J_m(c_{nf})\, e^{\sum_{n=1}^{N} im(n\omega t+\varphi_n-\gamma)}\, \mathrm{V(r)} d^3rdt + \int\int \frac{k_{ef}\nabla \mathrm{T_f}\exp(-\mathrm{i}\omega_{\mathrm{eTf}}\mathrm{t})}{(2\pi)^{3/2}} exp\{ip_i rcos\theta - iE_i t\} \sum_m^{\infty} J_m(c_{ni})\, e^{\sum_{n=1}^{N} im(n\omega t+\varphi_n-\gamma)}\, \mathrm{V(r)} d^3rdt - \int\int k_{ef}k_{ei}\nabla \mathrm{T_f}\nabla \mathrm{T_i}\exp\,(\mathrm{i}\omega_{\mathrm{eTi}}\mathrm{t} - \mathrm{i}\omega_{\mathrm{eTf}}\mathrm{t})\mathrm{V(r)} d^3rdt \quad (10)$$

Also, assuming $\sum_{n=1}^{N} n\omega = \omega_p$, expand $\Delta E = E_f - E_i$ from equation (10) we have

$$S = \delta_{fi} - e^{\sum_{n=1}^{N} i(\varphi_n-\gamma)} J_1(c_{nf}) \int\int \frac{1}{(2\pi)^2} e^{-iqrcos\theta}\, e^{i(E_f+\omega_p-E_i)t} \mathrm{V(r)} d^3rdt + e^{\sum_{n=1}^{N} i(\varphi_n-\gamma)} J_1(c_{nf}) k_{ei}\nabla \mathrm{T_i} \int\int e^{i(\omega_{\mathrm{eTi}}+E_f+\omega_p)t} e^{-ip_f rcos\theta} \mathrm{V(r)} d^3rdt + e^{\sum_{n=1}^{N} i(\varphi_n-\gamma)} J_1(c_{ni}) k_{ef}\nabla \mathrm{T_f} \int\int \frac{\mathrm{e}^{i(-\omega_{\mathrm{eTf}}-E_i+\omega_p)t}}{(2\pi)^{3/2}} e^{ip_i rcos\theta} \mathrm{V(r)} d^3rdt - k_{ef}k_{ei}\nabla \mathrm{T_f}\nabla \mathrm{T_i} \int\int \mathrm{e}^{\mathrm{i}(\omega_{\mathrm{eTi}}\mathrm{t}-\mathrm{i}\omega_{\mathrm{eTf}})\mathrm{t}}\, \mathrm{V(r)} d^3rdt \quad (11)$$

Taking Dirac dela for time integral from equation (11) we have

$$S = \delta_{fi} - e^{\sum_{n=1}^{N} i(\varphi_n-\gamma)} J_1(c_{nf}) 2\pi\delta(E_f + \omega_p - E_i) \frac{1}{(2\pi)^2} \int e^{-iqrcos\theta}\, \mathrm{V(r)} d^3r + e^{\sum_{n=1}^{N} i(\varphi_n-\gamma)} J_1(c_{nf}) k_{ei}\nabla \mathrm{T_i}\delta(\omega_{\mathrm{eTi}} + E_f + \omega_p) \int\int e^{-ip_f rcos\theta} \mathrm{V(r)} d^3r + \frac{1}{(2\pi)^{3/2}} e^{\sum_{n=1}^{N} i(\varphi_n-\gamma)} J_1(c_{ni}) k_{ef}\nabla \mathrm{T_f} 2\pi\delta(\omega_p - \omega_{\mathrm{eTf}} - E_i) \int e^{ip_i rcos\theta} \mathrm{V(r)} d^3r - k_{ef}k_{ei}\nabla \mathrm{T_f}\nabla \mathrm{T_i} 2\pi\delta(\omega_{\mathrm{eTi}}\mathrm{t} - \mathrm{i}\omega_{\mathrm{eTf}}) \int \mathrm{V(r)} d^3r \quad (12)$$

$$S = \delta_{fi} - e^{\sum_{n=1}^{N} i(\varphi_n - \gamma)} J_1(c_{nf}) 2\pi\delta(E_f + \omega_p - E_i) \frac{2\pi}{iq(2\pi)^2} \int \left(e^{-iqrcos\theta} - e^{-iqr}\right) \mathrm{V(r)} r\, dr + e^{\sum_{n=1}^{N} i(\varphi_n - \gamma)} J_1(c_{nf}) k_{ei} \nabla \mathrm{T_i} \delta(\omega_{\mathrm{eTi}} + E_f + \omega_p) \frac{2\pi}{ip_f} \int \left(e^{-ip_f rcos\theta} - e^{-ip_f r}\right) \mathrm{V(r)} r dr + \frac{1}{(2\pi)^{3/2}} e^{\sum_{n=1}^{N} i(\varphi_n - \gamma)} J_1(c_{ni}) k_{ef} \nabla \mathrm{T_f} 2\pi\delta(\omega_p - \omega_{\mathrm{eTf}} - E_i) \frac{2\pi}{ip_i} \int \left(e^{ip_i r} - e^{ip_i rcos\theta}\right) \mathrm{V(r)} r dr - k_{ef} k_{ei} \nabla \mathrm{T_f} \nabla \mathrm{T_i} 2\pi\delta(\omega_{\mathrm{eTi}} \mathrm{t} - \mathrm{i}\omega_{\mathrm{eTf}}) 2\pi(1 - cos\theta) \int \mathrm{V(r)} r^2 dr \qquad (13)$$

Now taking the potential $V(r)\left[-\frac{8}{r} - \frac{1}{|r-R_{OH_1}|} - \frac{1}{|r-R_{OH_2}|} + \sum_{i=i}^{10} \frac{1}{|r-r_i|}\right]$ and solving the radial part, from equation (13) we have

$$\int \left(e^{-iqrcos\theta} - e^{-iqr}\right) \mathrm{V(r)} r\, dr = \frac{8}{iq}\left(e^{-iqr} - \frac{e^{-iqrcos\theta}}{cos\theta}\right) - \left[R_{OH_1} e^{-iR_{OH_1} qcos\theta} Ei\left(iqcos\theta\left[R_{OH_1} - r\right]\right) + \frac{ie^{-iR_{OH_1} qcos\theta}}{qcos\theta} - R_{OH_1} e^{-iR_{OH_1} q} Ei\left(iq\left[R_{OH_1} - r\right]\right) \frac{ie^{-iR_{OH_1} q}}{q}\right] - \left[R_{OH_2} e^{-iR_{OH_2} qcos\theta} Ei\left(iqcos\theta\left[R_{OH_2} - r\right]\right) + \frac{ie^{-iR_{OH_2} qcos\theta}}{qcos\theta} - R_{OH_2} e^{-iR_{OH_2} q} Ei\left(iq\left[R_{OH_2} - r\right]\right) \frac{ie^{-iR_{OH_2} q}}{q}\right] + \sum_{i=i}^{10} \left[r_i\, e^{-ir_i qcos\theta} Ei\left(iqcos\theta[r_i - r]\right) + \frac{ie^{-ir_i qcos\theta}}{qcos\theta} - r_i\, e^{-ir_i q} Ei\left(iq[r_i - r]\right) \frac{ie^{-ir_i q}}{q}\right] \qquad (13a)$$

$$\int \left(e^{-ip_f r\cos\theta} - e^{-ip_f r}\right)\mathrm{V(r)}rdr$$
$$= \frac{8}{ip_f}\left(e^{-ip_f r} - \frac{e^{-ip_f r\cos\theta}}{\cos\theta}\right)$$
$$- \left[R_{OH_1}\, e^{-iR_{OH_1}p_f\cos\theta} Ei\left(ip_f\cos\theta\left[R_{OH_1} - r\right]\right) + \frac{ie^{-iR_{OH_1}p_f\cos\theta}}{p_f\cos\theta}\right.$$
$$\left. - R_{OH_1}\, e^{-iR_{OH_1}p_f} Ei\left(ip_f\left[R_{OH_1} - r\right]\right)\frac{ie^{-iR_{OH_1}p_f}}{p_f}\right]$$
$$- \left[R_{OH_2}\, e^{-iR_{OH_2}p_f\cos\theta} Ei\left(ip_f\cos\theta\left[R_{OH_2} - r\right]\right) + \frac{ie^{-iR_{OH_2}p_f\cos\theta}}{p_f\cos\theta}\right.$$
$$\left. - R_{OH_2}\, e^{-iR_{OH_2}p_f} Ei\left(ip_f\left[R_{OH_2} - r\right]\right)\frac{ie^{-iR_{OH_2}p_f}}{p_f}\right]$$
$$+ \sum_{i=i}^{10}\left[r_i\, e^{-ir_i p_f\cos\theta} Ei\left(ip_f\cos\theta[r_i - r]\right) + \frac{ie^{-ir_i p_f\cos\theta}}{p_f\cos\theta}\right.$$
$$\left. - r_i\, e^{-ir_i p_f} Ei\left(ip_f[r_i - r]\right)\frac{ie^{-ir_i p_f}}{p_f}\right] \qquad (13b)$$

$$\int \left(e^{-ip_i r\cos\theta} - e^{-ip_i r}\right)\mathrm{V(r)}rdr$$
$$= \frac{8}{ip_i}\left(e^{-ip_i r} - \frac{e^{-ip_i r\cos\theta}}{\cos\theta}\right)$$
$$- \left[R_{OH_1}\, e^{-iR_{OH_1}p_i\cos\theta} Ei\left(ip_i\cos\theta\left[R_{OH_1} - r\right]\right) + \frac{ie^{-iR_{OH_1}p_i\cos\theta}}{p_i\cos\theta}\right.$$
$$\left. - R_{OH_1}\, e^{-iR_{OH_1}p_i} Ei\left(ip_i\left[R_{OH_1} - r\right]\right)\frac{ie^{-iR_{OH_1}p_i}}{p_i}\right]$$
$$- \left[R_{OH_2}\, e^{-iR_{OH_2}p_i\cos\theta} Ei\left(ip_i\cos\theta\left[R_{OH_2} - r\right]\right) + \frac{ie^{-iR_{OH_2}p_i\cos\theta}}{p_i\cos\theta}\right.$$
$$\left. - R_{OH_2}\, e^{-iR_{OH_2}p_i} Ei\left(ip_i\left[R_{OH_2} - r\right]\right)\frac{ie^{-iR_{OH_2}p_i}}{p_i}\right]$$
$$+ \sum_{i=i}^{10}\left[r_i\, e^{-ir_i p_i\cos\theta} Ei\left(ip_i\cos\theta[r_i - r]\right) + \frac{ie^{-ir_i p_i\cos\theta}}{p_i\cos\theta}\right.$$
$$\left. - r_i\, e^{-ir_i p_i} Ei\left(ip_i[r_i - r]\right)\frac{ie^{-ir_i p_i}}{p_i}\right] \qquad (13c)$$

$$\int \mathrm{V(r)}r^2 dr = -4r^2 - \left[\frac{r^2}{2} + R_{OH_1}r + R_{OH_1}^2\log\left(r - R_{OH_1}\right)\right]$$
$$- \left[\frac{r^2}{2} + R_{HO_2}r + R_{OH_2}^2\log\left(r - R_{OH_2}\right)\right]$$
$$+ \left[\sum_{i=i}^{10}\frac{r^2}{2} + r_i r + r_i^2\log(r - r_i)\right] \qquad (13d)$$

On substituting all value of integration form equation 13(a) to equation 13(d) in equation (13) we get final S-matrix and S-matrix and T matrix (Kroll and Watson, 1973) we have from equation (6) as .

$$T_{fi} = \frac{i}{\hbar}\int_{-\infty}^{+\infty} \langle X_f(r,t)|V(r)|X_i(r,t)\rangle \, dt \tag{14}$$

Also, we have relation between differential cross-section and T-matrix (Kavazović et al., 2021).

$$\frac{d\sigma}{d\Omega} = \frac{p_f}{p_i} \left|T_{fi}\right|^2 \tag{15}$$

Now putting value of T_{fi} from equation (14) in equation(15) we get DCS. The developed model is used to investigate the scattering behavior of electrons interacting with water (H_2O) molecules under different thermal (293–300 K) and non-thermal (0 K) conditions. The framework incorporates laser-assisted effects through a thermally modified Volkov wave function and employs potential of H_2O molecule. By varying parameters such as scattering angle, momentum transfer, field strength, polarization, and Bessel function order, the model allows detailed analysis of DCS, resonance features, and interference patterns, highlighting the combined influence of thermal and laser fields on electron-molecule interactions.

3. Results and Discussion

Figure 1 is computed for a distance separation of 1 Å with parameters: photon number 2, relative field strength 2 a.u., absolute field strength 1.5 a.u., initial electron conductivity 10 a.u., final electron conductivity 0.15 a.u., initial temperature (∇T_i) 293 K, and final electron temperature (∇T_f) 300 K. The results show that the interacting nature or probability of scattering of e-H_2O at a scattering angle of 5.7° remains nearly constant, indicating that the electrostatic interaction energy is comparable to the rest energy of the scattering particles. In terms of polarization, the DCS is highest for circular, followed by elliptical, and then linear polarization, as illustrated in Figure 1(a). At a reduced scattering angle of 0.57°, slight resonances are observed around 0.25 eV and 1 eV, while further decreasing the angle to 0.057° produces stronger resonances with higher amplitudes but lower DCS values. These findings demonstrate that the scattering angle plays a crucial role in to study the nature of e-H_2O variation at specific momentum changes (Dhobi et al., 2025b), exhibiting damping-like behavior due to the nature of the Bessel function. Moreover, the peak seen in Figure 1(c) is associated with the self-healing property of the Bessel function, which tends to restore oscillatory patterns after energy loss, emphasizing the combined influence of angular dependence and Bessel-function dynamics on scattering behavior.

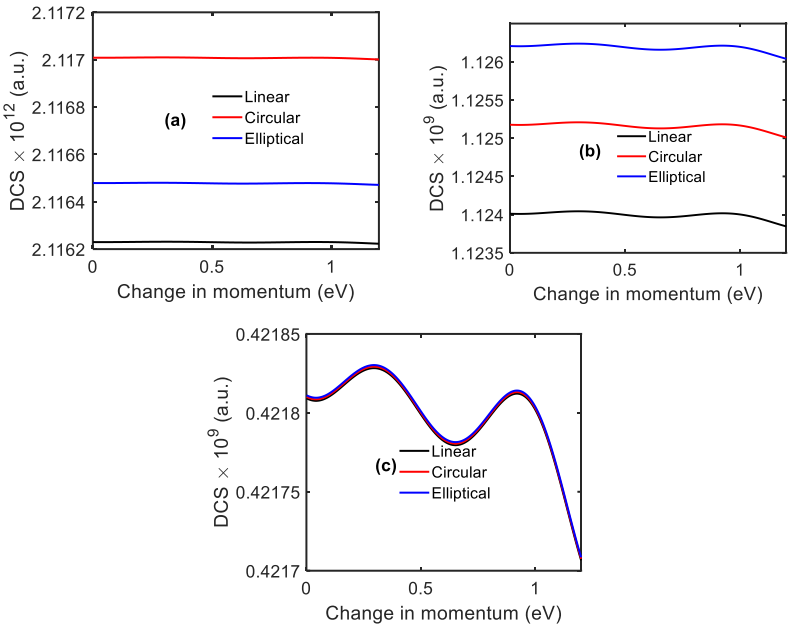

Figure 1: DCS with change in momentum (a)=5.7°, (b) 0.57°, (c)=0.057° at ∇T_i=293K and ∇T_f=300K

Figure 2 is computed for a distance separation of 1 Å at a scattering angle of 0.57°, with parameters set as photon number n=2, relative field strength 0.5 a.u., absolute field strength 0.5 a.u., initial electron conductivity (k_{ei}) 10 a.u. and final electron conductivity (k_{ef}) 0.15 a.u. The results show that at a scattering angle of 5.7 °, when temperature is considered zero in Equation (15), the probability of interaction of e-H_2O increases with momentum transfer, indicating that in the non-thermal case the temperature contribution is effectively negated. However, when thermal conditions are included (∇T_i =293K and ∇T_f=300 K), the interaction of e-H_2O is consistently higher than in the non-thermal case (∇T_i=∇T_f=0 K). This demonstrates that temperature has a significant role in enhancing scattering, as the thermal environment contributes additional electron oscillations that increase scattering probability. The nature of variation also differs under specific parameters, with increases in e-H_2O interaction corresponding to resonances at certain momentum or energy values. These findings suggest that temperature not only assists scattering in a similar way to laser-assisted processes but also provides an additional mechanism for manipulating electron–particle interactions, thereby increasing the likelihood of scattering events. Das and Dhobi (2025) show the similar nature when they study Scattering Dynamics with Gaussian Potential in the Presence of a Bichromatic Laser Field.

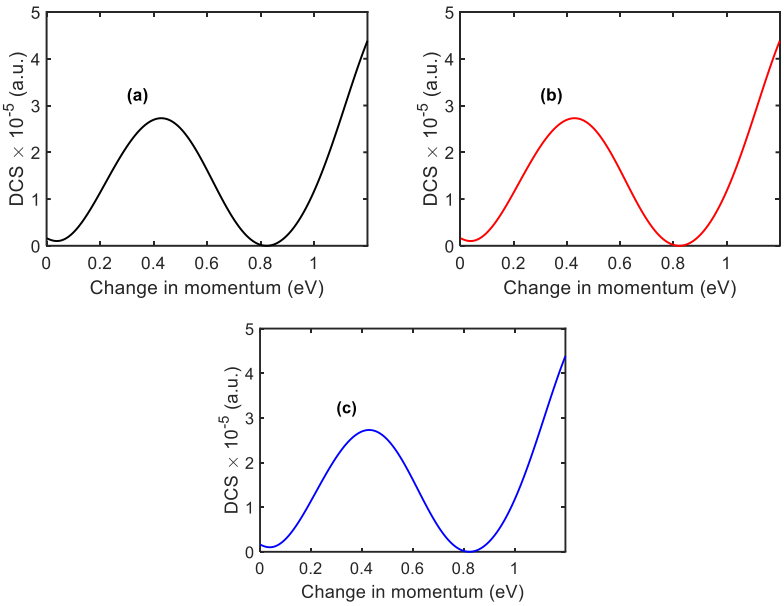

Figure 2: DCS with change in momentum (a) linear (b) circular, (c) elliptical at 5.7° and 0 K

To compute the results shown in Figure 3, we consider momentum transfer of 0.4 eV, a scattering angle of 5.7°, relative field strength of 1 a.u., field strength of 0.4 a.u., with ., initial electron conductivity of 10 a.u. and final electron conductivity of 15 a.u. The figure presents the variation of DCS with distance separation, where stronger fluctuations are observed for the thermal case (Figure 3a) compared to the non-thermal case (Figure 3b). The enhanced oscillations of e-H_2O in the thermal case arise from the combined effects of temperature-induced resonance and superposition, which increase both the field energy and amplitude, since amplitude is directly dependent on e-H_2O scattering. As a result, a strong fluctuation is observed around 2.2 Å in Figure 3(a). Below this distance, the DCS increases smoothly but very slowly, whereas beyond 2.2 Å it decreases gradually and eventually approaches a constant value. The constant nature of DCS in this regime is attributed to the electrostatic interaction energy becoming equal to the rest energy of the scattering particles. Furthermore, the DCS under thermal conditions is consistently higher than in the non-thermal case when other parameters are kept the same. A comparison across polarizations shows that elliptical polarization yields slightly higher DCS values than circular polarization, while circular polarization remains marginally higher than linear polarization.

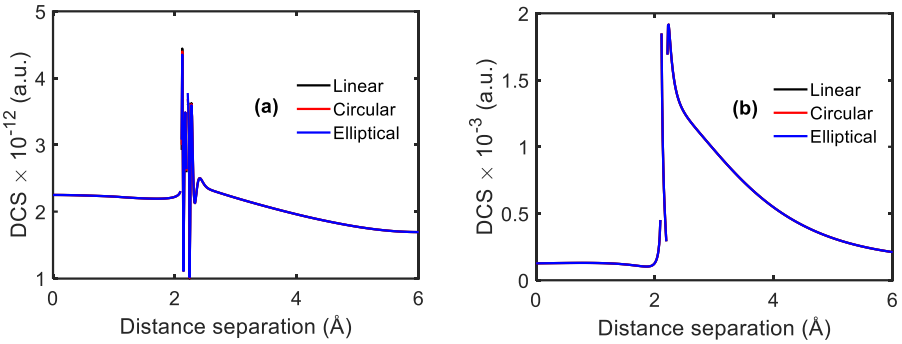

Figure 3: DCS with separation distance (a) ∇T_i=293K and ∇T_f=300K , (b) $\nabla T_i = \nabla T_f$=0K

Figure 4 is computed for a distance separation of 1.5 Å, momentum transfer of 1 eV, relative field strength of 0.3 a.u., absolute field strength of 5 a.u., initial electron conductivity of 0.1 a.u., and final electron conductivity of 0.5 a.u. The results show that the e-H_2O exhibits distinct behaviors under thermal and non-thermal conditions, with the thermal case consistently producing higher values than the non-thermal case. In Figure 4(a), two sharp peaks are observed: the upper peak arises from strong resonance and constructive interference, while the lower peak is associated with destructive interference. When electron conductivity decreases, the nature of interaction between the projectile and the target changes, leading to modifications in the DCS amplitude, which is found to decrease as shown in Figure 4(b). The peak in Figure 4(b) is again due to constructive interference, whereas the regions where the e-H_2O scattering becomes constant indicate that the electrostatic interaction energy has reached equilibrium with the rest energy of the scattering particles, implying that no further approach of the projectile to the target occurs. In Figure 4(c), the DCS decreases with increasing scattering angle, accompanied by a reduction in amplitude. Although the overall trends remain similar across all polarization cases, the magnitude of DCS is slightly higher for circular polarization compared to elliptical, while elliptical polarization remains marginally higher than linear.

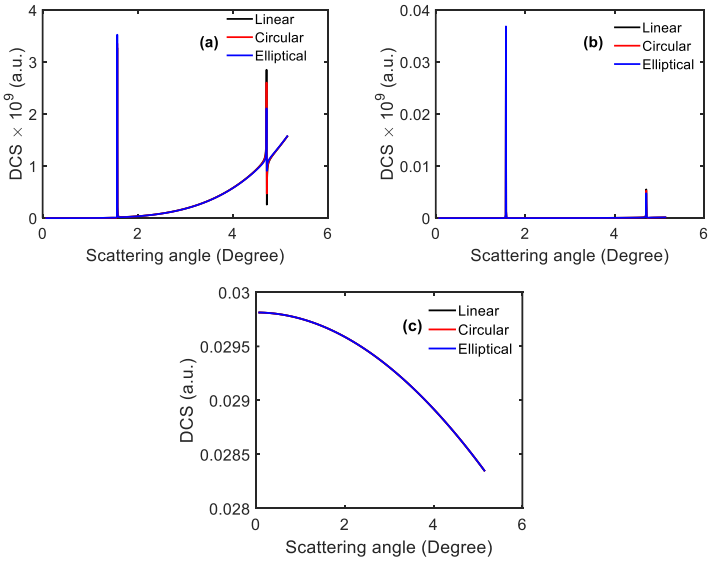

Figure 4: DCS with scattering angle (a) k_{ei}=0.1 a.u. k_{ef}=0.5 a.u., (b) k_{ei} = 0.01 a. u., k_{ef}=0.05 a.u. at $\nabla T_i = 293\ K, \nabla T_f = 300\ K$ (c) $\nabla T_i = \nabla T_f = 0K$

Figure 5 is computed for momentum transfer of 1 eV, separation distance of 1.5 Å, scattering angle of 57°, relative field strength of 2.5 a.u., field strength of 0.9 a.u., with initial electron conductivity of 0.10 a.u. and final electron conductivity of 0.5 a.u. Figure 5(a) shows that the e-H_2O scattering increases with increasing temperature, while Figure 5(b) demonstrates a similar trend of increasing e-H_2O interacting with increasing field strength. In both cases, the overall nature of the curves remains consistent across all polarization states, with slight differences in magnitude: elliptical polarization yields the highest DCS, followed by circular, and then linear polarization. These results indicate that both temperature and field strength enhance the scattering probability by increasing electron oscillations, which in turn raise the DCS amplitude. In addition, Dhobi et al. (2026; 2025c) shows that DCS has effect on temperature.

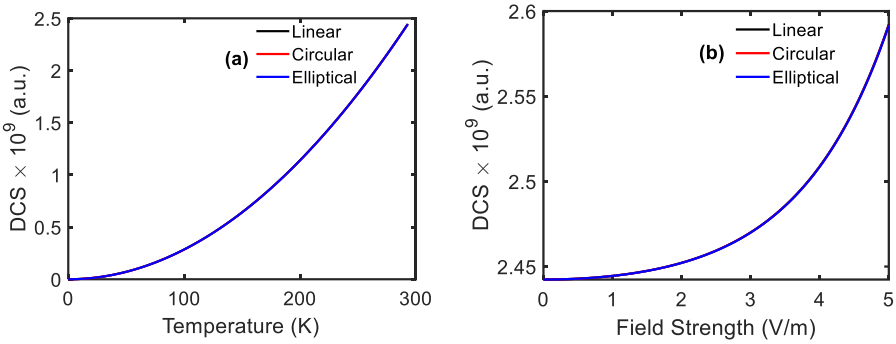

Figure 5: DCS with temperature (a) with $\nabla T_f = 300K$ and (b) field strength

Figure 6 is computed for distance separation 1.5 and monetum transformation 0.3 eV, scattering angle 5.7°, relative field strength 2.5 a.u., absolute field strength 0.9 a.u., with initial electron conductivity of 0.10 a.u. and final electron conductivity of 0.5 a.u. The results show that the e-H_2O probability of scattering decreases with increasing order of the Bessel function across all scattering angles. At higher scattering angles, the DCS is relatively larger, whereas at lower angles it is significantly reduced. Moreover, as the scattering angle decreases, the e-H_2O scattering probability values for different polarization states gradually converge, as illustrated in Figure 6(c), with elliptical polarization showing the strongest convergence trend. At lower Bessel orders, the DCS is distinguishable between polarization cases, while at higher orders the differences diminish and the polarization dependence becomes negligible. For very high Bessel orders, the DCS approaches an almost constant value, which indicates that the electrostatic interaction energy and the rest energy of the scattering particles reach equilibrium. This behavior highlights the damping-like nature of higher-order Bessel modes, where oscillatory effects are suppressed, leading to a saturation in the scattering cross-section.

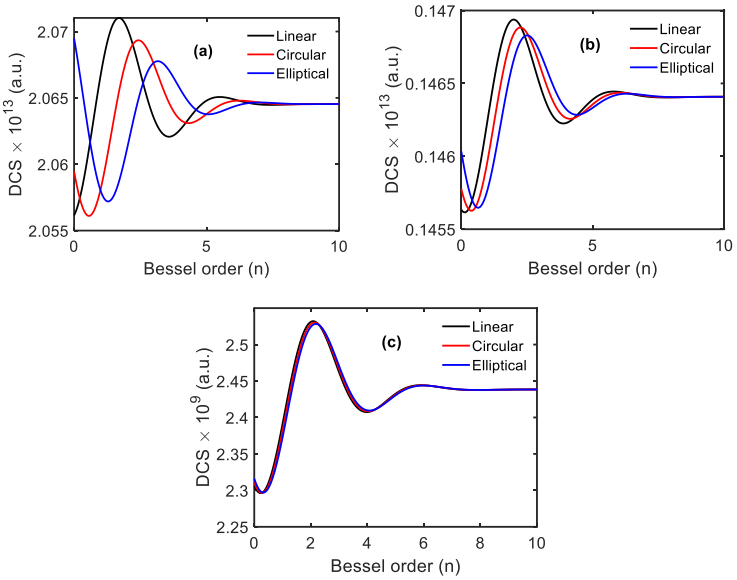

Figure 6: DCs with Bessel function (a) 57°, (b) 28°, (c) 5.7° at $\nabla T_i = 293$ K and $\nabla T_f = 300$K

4. Conclusion

The results demonstrate that the e-H_2O DCS in laser-assisted electron–quantum dot scattering is strongly influenced by temperature, scattering angle, field strength, polarization, distance separation, and Bessel function order. Thermal effects consistently enhance e-H_2O DCS compared to non-thermal conditions, as increased electron oscillations raise scattering probability. Resonances are observed at specific momentum or energy values, particularly at lower scattering angles, while higher angles generally exhibit larger e-H_2O DCS. Polarization affects scattering magnitude, with elliptical polarization producing the highest DCS, followed by circular and linear. Variation in distance separation and electron conductivity modulates e-H_2O DCS amplitude, revealing constructive and destructive interference patterns. Increasing field strength and temperature further amplifies scattering, highlighting the combined role of external fields and thermal excitation. Higher-order Bessel functions reduce polarization dependence and produce nearly constant DCS, reflecting the balance between electrostatic interaction energy and particle rest energy. Overall, these findings illustrate the interplay of thermal, field, and geometric factors in controlling electron-QD scattering.

Acknowledgment: The authors would like to thank the Department of Physics, Patan Multiple Campus, Lalitpur, Tribhuvan University and Department of Physics, Golden gate international college, Tribhuvan University, Kathmandu, Nepal for providing possible reserch facilities to conduct this research.

References

Bartschat, K., & Kushner, M. J. (2016). Electron collisions with atoms, ions, molecules, and surfaces: Fundamental science empowering advances in technology. *Proceedings of the National Academy of Sciences*, *113*(26), 7026-7034.

De Avillez, M. A., Guerra, M., Santos, J. P., & Breitschwerdt, D. (2019). Relativistic electron impact ionization cross sections of carbon ions and application to an optically thin plasma. *Astronomy & Astrophysics*, *631*, A42.

Campeanu, R. I., Walters, H. R. J., & Whelan, C. T. (2018). Electron-and positron-impact ionization of inert gases. *Physical Review A*, *97*(6), 062702.

Colgan, J., Pindzola, M. S., Robicheaux, F. J., Griffin, D. C., & Baertschy, M. (2002). Time-dependent close-coupling calculations of the triple-differential cross section for electron-impact ionization of hydrogen. *Physical Review A*, *65*(4), 042721.

Ehlotzky, F. (2001). Atomic phenomena in bichromatic laser fields. *Physics Reports*, *345*(4), 175-264.

Zarcone, M., Moores, D. L., & McDowell, M. R. C. (1983). Laser-assisted electron impact ionisation of helium at 256.5 ev. *Journal of Physics B: Atomic and Molecular Physics*, *16*(2), L11.

Khalil, D., Maquet, A., Taïeb, R., Joachain, C. J., & Makhoute, A. (1997). Laser-assisted (e, 2 e) collisions in helium. *Physical Review A*, *56*(6), 4918.

Batra, K., Kundliya, R., & Mohan, M. (2004). Atom in a femtosecond bichromatic laser field. *Pramana*, *62*(1), 31-36.

Milosevic, D. B. (1996). Potential scattering in a strong multicolour laser field. *Journal of Physics B: Atomic, Molecular and Optical Physics*, *29*(4), 875.

Luo, S., Li, M., Xie, H., Zhang, P., Xu, S., Li, Y., ... & Lu, P. (2017). Angular-dependent asymmetries of above-threshold ionization in a two-color laser field. *Physical Review A*, *96*(2), 023417.

Maurer, J., and Keller, U. (2021). Ionization in intense laser fields beyond the electric dipole approximation: concepts, methods, achievements and future directions. Journal of Physics B: Atomic, Molecular and Optical Physics, 54(9)

Ehlotzky, F. (2001). *Atomic phenomena in bichromatic laser fields. Physics Reports, 345(4), 175–264.* doi:10.1016/s0370-1573(00)00100-9

Kroll, N.M. and Watson, K.M. (1973). Charged-particle scattering in the presence of a strong electromagnetic wave. Physical Review A, 8: 804–809.

Kavazović, K., Čerkić, A., & Milošević, D. B. (2021). Electron-molecule scattering in a bichromatic elliptically polarised laser field: Plateau structures and two-centre interference minima. *Molecular Physics*, *119*(14), e1948123

Dhobi, S. H., Yadav, K., Gupta, S. P., Nakarmi, J. J., & Jha, A. K. (2026). Temperature dependence laser-assist scattering and its impact on efficiency of PEMFC. *PLoS One*, *21*(1), e0336352.

Dhobi, S. H., Yadav, K., Gupta, S. P., Nakarmi, J. J., & Jha, A. K. (2025c). Influence of Scattering Dynamics on Efficiency of Proton Exchange Membrane Fuel Cell. *Fuel Cells*, *25*(6), e70039.

Dhobi, S. H., Gupta, S. P., Yadav, K., Nakarmi, J. J., & Jha, A. K. (2025b). Thermal Electron-Hydrogen Laser Assisted Three-Body Scattering Dynamics. *Physics Open*, 100328.

Kurmi, R. P., Yadav, K., Shrestha, A., & Dhobi, S. H. (2025). Laser assist quantum dot scattering with Gaussian potential. *Physics Open*, *23*, 100267.

Dhobi, S. H., Yadav, K., Gupta, S. P., Nakarmi, J. J., & Jha, A. K. (2025a). Non-monochromatic laser assist scattering in thermal environment. *Journal of the Nigerian Society of Physical Sciences*, 2345-2345.

Das, S. K., & Dhobi, S. H. (2025). Scattering Dynamics with Gaussian Potential in the Presence of a Bichromatic Laser Field. *Api Journal of Science*, *2*, 40-47.